Supporting Information

Alloy-induced phase transition and enhanced photovoltaic performance: The case of $Cs_3Bi_2I_{9-x}Br_x$ perovskite solar cells

Bin-Bin Yu,[a,b†] Min Liao,[a,c†] Jingxiu Yang,[d†] Wei Chen,[a] Yudong Zhu,[a] Xusheng Zhang,[a] Tao Duan,[c] Weitang Yao,[c*] Su-Huai Wei,[d*] and Zhubing He[a*]

[a] Department of Materials Science and Engineering, Shenzhen Key Laboratory of Full Spectral Solar Electricity Generation (FSSEG), Southern University of Science and Technology, No. 1088, Xueyuan Rd., Shenzhen, 518055, Guangdong, China.

[b] Academy for Advanced Interdisciplinary Studies, Southern University of Science and Technology, No. 1088, Xueyuan Rd., Shenzhen, 518055, Guangdong, China.

[c] Laboratory of Fundamental Science on Nuclear Wastes and Environmental Safety, Southwest University of Science and Technology, No. 59, Qinglong Avenue, Mianyang, 621010, Sichuan, China

[d] Beijing Computational Science Research Center, Beijing 100193, China

[†] Equally contributed to this paper.

*Corresponding Authors: Z.B. hezb@sustc.edu.cn; S.H. suhuaiwei@csrc.ac.cn; W.T. wtyao@ustc.edu.cn

Experimental Section

Materials: Bismuth iodide (BiI_3), Bismuth bromide ($BiBr_3$), Cesium iodide (CsI), Chlorobenzene (CB), N, N-dimethylformamide (DMF) and Dimethyl sulfoxide (DMSO), Nickel acetate tetrahydrate ($Ni(CH_3COO)_2{\bullet}4H_2O$), Ethanol (20 proof grade), Ethanolamine ($NH_2CH_2CH_2OH$) (>99.5% purity grade) were obtained from Sigma-Aldrich and used as received. $PC_{61}BM$ was obtained from Lumtec.

Device Fabrication: 0.225 M various $Cs_3Bi_2I_{9-x}Br_x$ (x=1, 2, 3, 4, 6) precursor solutions were prepared by dissolving according CsI, BiI_3 and $BiBr_3$ in the mixed solvent of DMF and DMSO (V_{DMF}: V_{DMSO}=4:1). $Cs_3Bi_2Br_9$ precursor solution was prepared by dissolving according CsBr, BiI_3 and $BiBr_3$ in the mixed solvent of DMF and DMSO (V_{DMF}: V_{DMSO}=4:1). The above solutions were heated at 60 °C and stirred over 2 hours. NiO_x precursor solution was obtained by dissolving 248.8 mg $Ni(CH_3COO)_2{\bullet}4H_2O$ in 10 mL ethanol (20 proof grade) with 60 uL ethanolamine.

The patterned ITO glass substrates were cleaned for 20 minutes in an ultrasonic bath with acetone, isopropanol and ethanol respectively. NiO_x layer was deposited by spin coating at 2000 rpm for 40 seconds in the air, then followed by annealing at 300 °C for 1 hour.

Next, deposition of the $Cs_3Bi_2I_{9-x}Br_x$ films were performed in N_2 glovebox. The $Cs_3Bi_2I_{9-x}Br_x$ solutions with different content of Br were filtered and dropped onto glass/ITO/ PEDOT:PSS substrates with the speed of 3500 rpm for 50 s. The CB-free $Cs_3Bi_2I_{9-x}Br_x$ films were obtained after annealing at 200 °C for 10 min. The $Cs_3Bi_2I_{9-x}Br_x$ films with CB treatment were fabricated by drop-casting chlorobenzene solvent at the 10 s of the spinning process and following same annealing process. $PC_{61}BM$ layers were spin coated on perovskite films and annealed at 100 °C for 10 min. Then, 10 nm C_{60} and 5 nm BCP were evaporated on the top of $Cs_3Bi_2I_{9-x}Br_x$ films. Finally, 80 nm Ag was evaporated as top electrode through the shadow masks by thermal evaporation to finish the device fabrication.

Characterizations: X-ray diffraction (XRD) spectra were collected using Rigaku MiniFlex600 X-ray diffractometer (Cu Kα, 1.5406 Å). The absorption spectra were taken using a Shimadzu ultraviolet-visible spectrophotometer (UV-3600). Top-view and cross-section morphology of perovskite films were analyzed by TESCAN MIRA3 scanning electron microscope. The current density-voltage (J-V) curves were measured by a Keithley 2400 sourcemeter under AM1.5 spectrum (100 mW/cm^2) using the xenon arc lamp of an Oriel Sol3A solar simulator. Light intensity was calibrated using a monocrystalline Si-cell. The devices were measured in reverse scan from 1.2 V to -0.2 V with 0.1 mV intervals and 10 ms delay time, and forward scan from -0.2 V to 1.2 V with identical interval and delay time. The EQE spectra were recorded with by an Enli Technology (Taiwan) EQE measurement system (QE-R) with the calibration for light intensity by a standard single-crystal Si-cell. Room temperature PL spectra were measured by Spectrofluorometer (FS5, Edinburgh instruments) with 405 nm pulsed laser.

Computational methods: Density functional theory (DFT) calculations were performed within the Perdew-Burke-Ernzerhof parametrization of the generalized gradient approximation, as implemented in the Vienna ab initio simulation package (VASP). The project augmented wave (PAW) method and the plane wave basis set are employed with an energy cutoff of 350 eV. All the atoms and the lattice vectors are fully relaxed until the force on each atom is less than 0.01 eV/Å. For the Brilloin zone integration, we used the $6\times6\times2$ and $6\times6\times4$ k-point mesh for the $P6_3/mmc$ and $P\bar{3}m$ primitive cells, respectively. we have employed the PBE functional with spin-orbit-coupling (SOC). Given the fact that the calculated band gap by PBE+SOC is underestimated compare to experimental data, we have used scissor operator to compensate the band gap error.

Figure S1

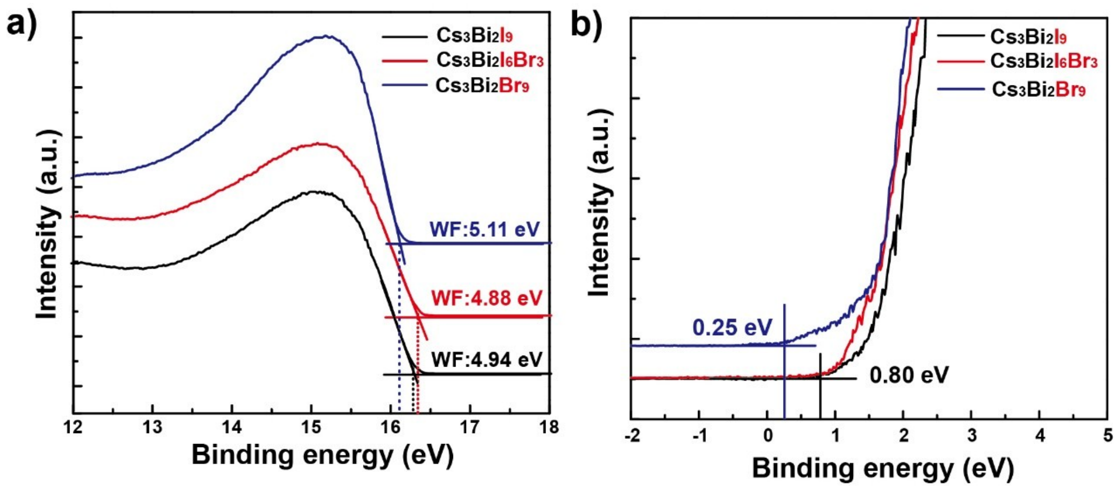

Figure S1. a, b) UPS spectra $Cs_3Bi_2I_9$, $Cs_3Bi_2I_6Br_3$ and $Cs_3Bi_2Br_9$ films, respectively.

Figure S2

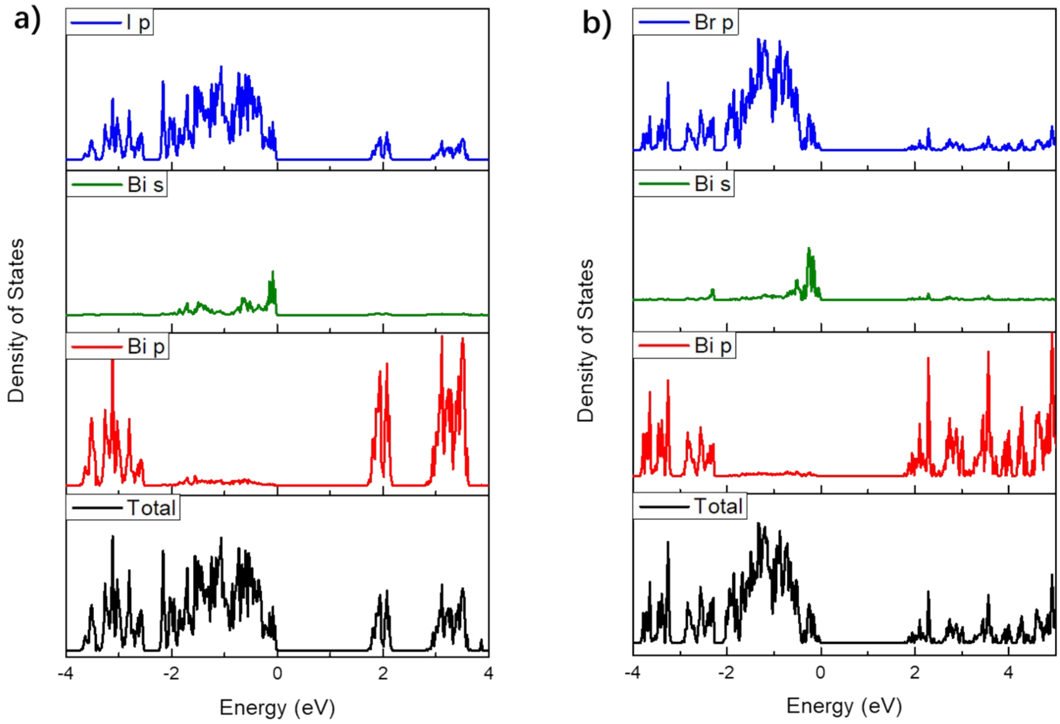

Figure S2. the projected density states for a) $Cs_3Bi_2I_9$ ($P6_3/mmc$) and b) $Cs_3Bi_2Br_9$ (P-3m) calculated by PBE+SOC approach.

Figure S3

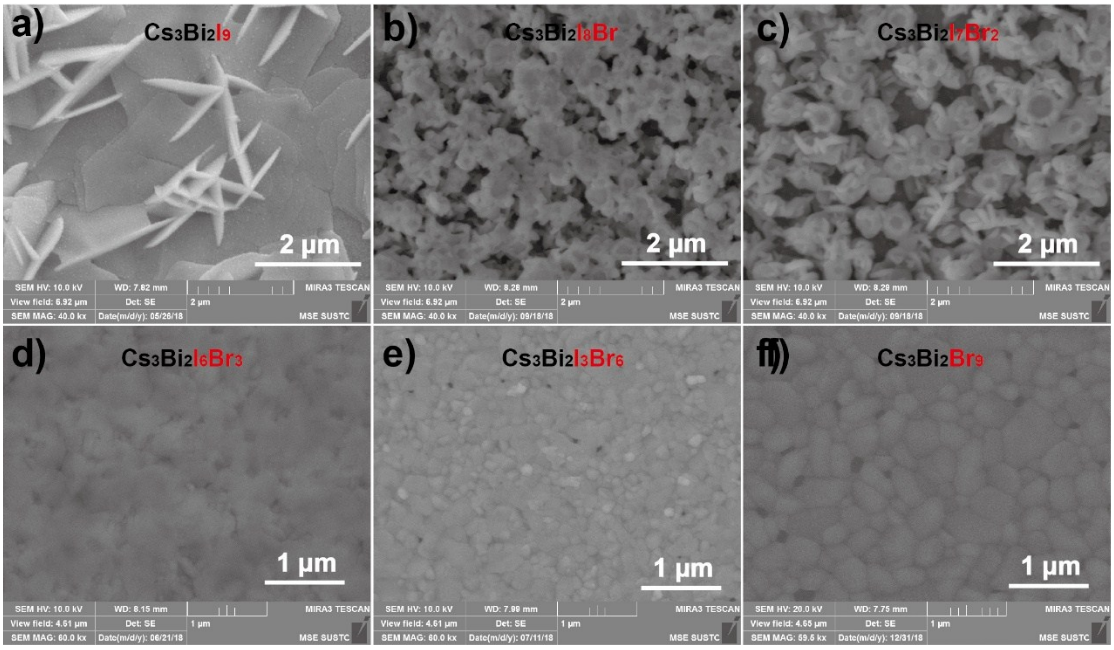

Figure S3. a-f) Top view SEM images of $Cs_3Bi_2I_{9-x}Br_x$ films with various Br contents.

Figure S4

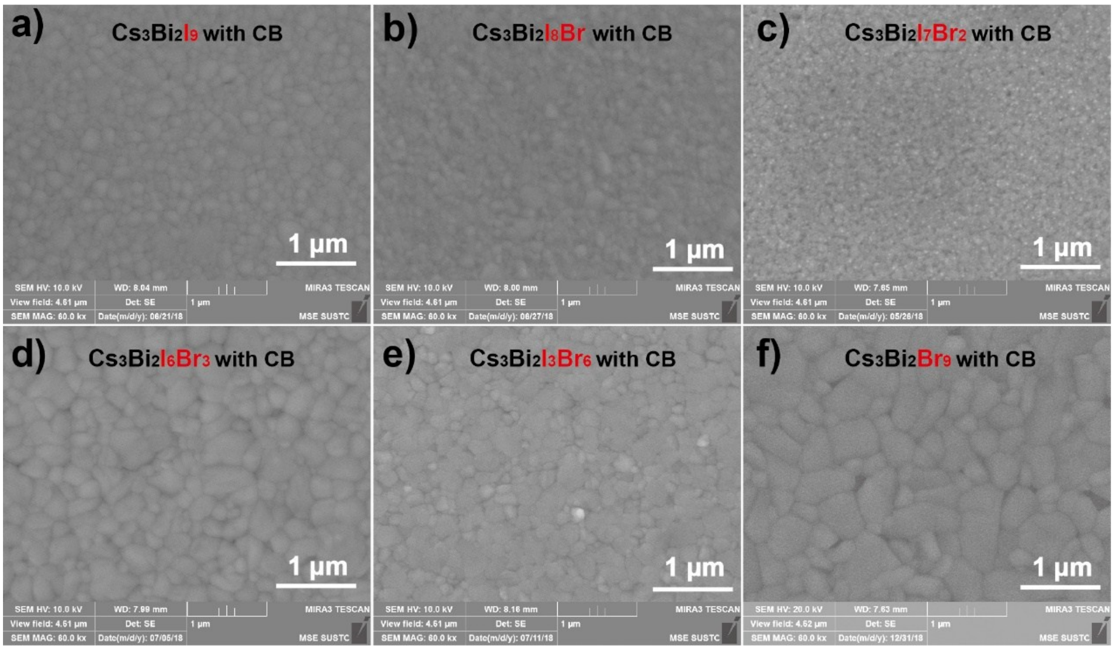

Figure S4. a-f) Top view SEM images of $Cs_3Bi_2I_{9-x}Br_x$ films with various Br contents by CB treatment.

Figure S5

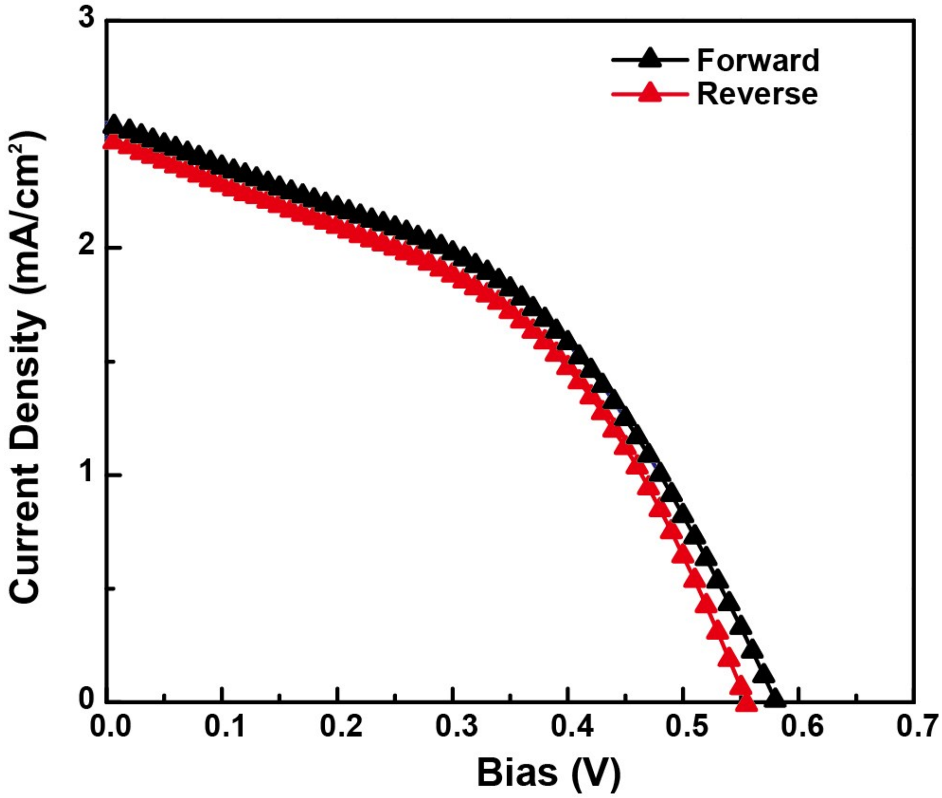

Figure S5. the J-V curves of champion devices for CB-free $Cs_3Bi_2I_6Br_3$ film.

Figure S6

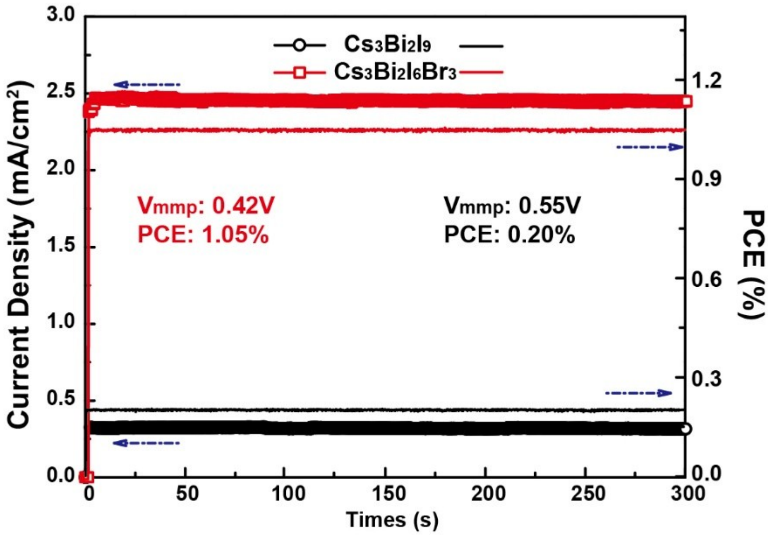

Figure S6. the steady photocurrent output at fixed bias of V_{mpp} and steady PCE of the corresponding optimal devices.

Table S1 the scissor operator estimated by the calculated band gap at Γ point.

	$Cs_3Bi_2I_9$ Gap(Γ-Γ)		$Cs_3Bi_2Br_9$ Gap (Γ-Γ)	
	$P6_3/mmc$	$P\bar{3}m$	$P6_3/mmc$	$P\bar{3}m$
PBE	2.43	2.00	3.22	2.71
PBE+SOC	1.89	1.42	2.63	1.94
SOC(scissor operator)	0.54	0.58	0.59	0.77

Table S2 the summary of progress of Bi-based PSCs.

Absorber	PCE (%)	V_{OC} (V)	J_{SC} (mA cm^{-2})	FF (%)	E_g (eV)	Architecture	Fabrication method	Ref.
$MA_3Bi_2I_9$	0.08	0.69	0.37	32	2.1	FTO/TiO_2/absorber/ spiro-OMeTAD/Ag	spin coating, gas-assisted	1
$MA_3Bi_2I_9$	0.42	0.67	1.00	63	2.1	ITO/TiO_2/mp-TiO_2/ absorber/spiro-OMeTAD/ MoO_3 /Ag	spin coating	2
$MA_3Bi_2I_9$	3.17	1.01	4.02	78	-	FTO/c-TiO_2/mp-TiO_2/ absorber/spiro-OMeTAD/ Au	evaporation	
$MA_3Bi_2I_9$	0.39	0.83	1.39	34	2.2	ITO/PEDOT:PSS/absorber/ C_{60}/BCP/Ag	evaporation spin-coating	3
$MA_3Bi_2I_9$	0.36	0.65	1.10	50	2.1	FTO/TiO_2/mp-TiO_2/ absorber/spiro-OMeTAD/Au	solvent-engineering spin-coating	4
$MA_3Bi_2I_9$	0.31	0.51	0.94	61	-	FTO/TiO_2/mpTiO_2/ absorber/spiro-OMeTAD/Au	spin coating	5
$MA_3Bi_2I_9$	0.26	0.56	0.83	49	-	FTO/TiO_2/mp-TiO_2/ absorber/spiro-OMeTAD/Au	spin coating	6
$MA_3Bi_2I_9$	0.19	0.35	1.16	46	2.1	FTO/TiO_2/mp-TiO_2/ absorber/P3HT/Au	spin coating	7
$MA_3Bi_2I_9$	0.12	0.68	0.52	33	2.1	FTO/TiO_2/mp-TiO_2/ absorber/spiro-OMeTAD/Ag	spin coating	8
$(MA_3Bi_2I_9)_{0.2}$ $(BiI_3)_{0.8}$	0.08	0.57	0.27	50	-	FTO/TiO_2/mp-TiO_2/ absorber/PTAA/PIDT-DFBT/Ag	spin coating	9
$Cs_3Bi_2I_9$	1.09	0.85	2.15	60	2.2	FTO/TiO_2/mp-TiO_2/ absorber/spiro-OMeTAD/Ag	spin coating	8

$Cs_3Bi_2I_9$	0.21	0.49	0.67	64	2.0	FTO/TiO_2/mp-TiO_2/ absorber/spiro-OMeTAD/Au	spin coating	10
$Cs_3Bi_2I_9$	3.20	0.86	5.78	64	2.3	FTO/TiO_2 / absorber/ CuI/Au	spin coating	11
$CsBi_3I_{10}$	0.40	0.31	3.40	38	1.77	FTO/TiO_2/mp-TiO_2/ absorber/P3HT/Ag	spin coating	12
$CsBi_3I_{10}$	1.51	0.46	4.75	69	1.77	FTO/TiO_2/absorber/Carbon	spin coating	13
$Cs_2AgBiBr_6$	2.43	0.98	3.93	63	2.21	FTO/c-TiO_2/mp-TiO_2/ absorber/spiro-OMeTAD/Au	spin coating	14
$Cs_2AgBiBr_6$	2.51	1.01	3.82	65	-	FTO/TiO_2/ $Cs_2AgBiBr_6$/ Spiro-OMeTAD/MoO_3/Ag	spin coating	15
$AgBi_2I_7$	1.22	0.56	3.30	67	1.87	FTO/TiO_2/mp-TiO_2/ absorber/P3HT/Ag	spin coating	16
Ag_2BiI_5	2.1	0.49	6.80	63	1.85	FTO/TiO_2/mp-TiO_2/ absorber/P3HT/Au	spin coating	17
Ag_2BiI_5	2.6	0.69	6.04	62	1.7	FTO/c-TiO_2/mp-TiO_2/ absorber/PTAA/Au	spin coating hot casting	18
$AgBiI_4$	0.89	0.84	2.37	45	1.86	FTO/TiO_2/ absorber/ P3HT/Au	spin coating	19
$Ag_3BiI_{5.92}S_{0.04}$	5.56	0.57	14.7	66	-	FTO/c-TiO_2/m-TiO_2/ absorber /PTAA/Au	spin coating air blowing	20
$C_5H_6NBiI_4$	0.9	0.62	2.71	54	1.98	FTO/c-TiO_2/mp-TiO_2/ absorber /ZrO_2/C	spin coating	21
$CuBiI_4$	0.82	0.63	2.19	57	2.67	FTO/TiO_2/ absorber/ Spiro-OMeTAD/Au	spin coating	22

References:

(1) Okano, T.; Suzuki, Y. Gas-assisted coating of Bi-based $(CH_3NH_3)_3Bi_2I_9$ active layer in perovskite solar cells. *Mater. Lett.* **2017,** *191*, 77-79.

(2) Zhang, X.; Wu, G.; Gu, Z.; Guo, B.; Liu, W.; Yang, S.; Ye, T.; Chen, C.; Tu, W.; Chen, H. Active-layer evolution and efficiency improvement of $(CH_3NH_3)_3Bi_2I_9$-based solar cell on TiO_2-deposited ITO substrate. *Nano Research* **2016,** *9* (10), 2921-2930.

(3) Ran, C.; Wu, Z.; Xi, J.; Yuan, F.; Dong, H.; Lei, T.; He, X.; Hou, X. Construction of Compact Methylammonium Bismuth Iodide Film Promoting Lead-Free Inverted Planar Heterojunction Organohalide Solar Cells with Open-Circuit Voltage over 0.8 V. *The Journal of Physical Chemistry Letters* **2017,** *8* (2), 394-400.

(4) Mali, S. S.; Kim, H.; Kim, D.-H.; Kook Hong, C. Anti-Solvent Assisted Crystallization Processed Methylammonium Bismuth Iodide Cuboids towards Highly Stable Lead-Free Perovskite Solar Cells. *ChemistrySelect* **2017,** *2* (4), 1578-1585.

(5) Kulkarni, A.; Singh, T.; Ikegami, M.; Miyasaka, T. Photovoltaic enhancement of bismuth halide hybrid perovskite by N-methyl pyrrolidone-assisted morphology conversion. *RSC Adv.* **2017,** *7* (16), 9456-9460.

(6) Singh, T.; Kulkarni, A.; Ikegami, M.; Miyasaka, T. Effect of Electron Transporting Layer on Bismuth-Based Lead-Free Perovskite $(CH_3NH_3)_3Bi_2I_9$ for Photovoltaic Applications. *ACS Appl. Mater. Interfaces* **2016,** *8* (23), 14542-14547.

(7) Lyu, M. Q.; Yun, J. H.; Cai, M. L.; Jiao, Y. L.; Bernhardt, P. V.; Zhang, M.; Wang, Q.; Du, A. J.; Wang, H. X.; Liu, G.; Wang, L. Z. Organic-inorganic bismuth (III)-based material: A lead-free, air-stable and solution-processable light-absorber beyond organolead perovskites. *Nano Research* **2016,** *9* (3), 692-702.

(8) Park, B. W.; Philippe, B.; Zhang, X. L.; Rensmo, H.; Boschloo, G.; Johansson, E. M. J. Bismuth Based Hybrid Perovskites $A_3Bi_2I_9$ (A: Methylammonium or Cesium) for Solar Cell Application. *Adv. Mater.* **2015,** *27* (43), 6806.
(9) Lan, C. F.; Luo, J. T.; Zhao, S.; Zhang, C.; Liu, W. G.; Hayase, S. Z.; Ma, T. L. Effect of lead-free $(CH_3NH_3)_3Bi_2I_9$ perovskite addition on spectrum absorption and enhanced photovoltaic performance of bismuth triiodide solar cells. *J. Alloy. Compd.* **2017,** *701*, 834-840.
(10) Ghosh, B.; Wu, B.; Mulmudi, H. K.; Guet, C.; Weber, K.; Sum, T. C.; Mhaisalkar, S.; Mathews, N. Limitations of $Cs_3Bi_2I_9$ as Lead-Free Photovoltaic Absorber Materials. *ACS Appl. Mater. Interfaces* **2018,** *10* (41), 35000-35007.
(11) Bai, F.; Hu, Y.; Hu, Y.; Qiu, T.; Miao, X.; Zhang, S. Lead-free, air-stable ultrathin $Cs_3Bi_2I_9$ perovskite nanosheets for solar cells. *Solar Energy Materials and Solar Cells* **2018,** *184*, 15-21.
(12) Johansson, M. B.; Zhu, H. M.; Johansson, E. M. J. Extended Photo-Conversion Spectrum in Low-Toxic Bismuth Halide Perovskite Solar Cells. *J. Phys. Chem. Lett.* **2016,** *7* (17), 3467-3471.
(13) Shin, J.; Kim, M.; Jung, S.; Kim, C. S.; Park, J.; Song, A.; Chung, K.-B.; Jin, S.-H.; Lee, J. H.; Song, M. Enhanced efficiency in lead-free bismuth iodide with post treatment based on a hole-conductor-free perovskite solar cell. *Nano Research* **2018,** *11* (12), 6283-6293.
(14) Greul, E.; Petrus, M. L.; Binek, A.; Docampo, P.; Bein, T. Highly stable, phase pure $Cs_2AgBiBr_6$ double perovskite thin films for optoelectronic applications. *J. Mater. Chem. A* **2017,** *5* (37), 19972-19981.
(15) Igbari, F.; Wang, R.; Wang, Z.-K.; Ma, X.-J.; Wang, Q.; Wang, K.-L.; Zhang, Y.; Liao, L.-S.; Yang, Y. Composition Stoichiometry of $Cs_2AgBiBr_6$ Films for Highly Efficient Lead-Free Perovskite Solar Cells. *Nano Letters* **2019,** *19* (3), 2066-2073.
(16) Kim, Y.; Yang, Z. Y.; Jain, A.; Voznyy, O.; Kim, G. H.; Liu, M.; Quan, L. N.; de Arquer, F. P. G.; Comin, R.; Fan, J. Z.; Sargent, E. H. Pure Cubic-Phase Hybrid Iodobismuthates $AgBi_2I_7$ for Thin-Film Photovoltaics. *Angew. Chem.-Int. Edit.* **2016,** *55* (33), 9586-9590.
(17) Zhu, H. M.; Pan, M. G.; Johansson, M. B.; Johansson, E. M. J. High Photon-to-Current Conversion in Solar Cells Based on Light-Absorbing Silver Bismuth Iodide. *ChemSusChem* **2017,** *10* (12), 2592-2596.
(18) Ghosh, B.; Wu, B.; Guo, X.; Harikesh, P. C.; John, R. A.; Baikie, T.; Arramel; Wee, A. T. S.; Guet, C.; Sum, T. C.; Mhaisalkar, S.; Mathews, N. Superior Performance of Silver Bismuth Iodide Photovoltaics Fabricated via Dynamic Hot-Casting Method under Ambient Conditions. *Advanced Energy Materials* **2018,** *8* (33), 1802051.
(19) Khazaee, M.; Sardashti, K.; Chung, C.-C.; Sun, J.-P.; Zhou, H.; Bergmann, E.; Dunlap-Shohl, W. A.; Han, Q.; Hill, I. G.; Jones, Jacob L.; Lupascu, D. C.; Mitzi, D. B. Dual-source evaporation of silver bismuth iodide films for planar junction solar cells. *J. Mater. Chem. A* **2019,** *7* (5), 2095-2105.
(20) Pai, N.; Lu, J.; Gengenbach, T. R.; Seeber, A.; Chesman, A. S. R.; Jiang, L.; Senevirathna, D. C.; Andrews, P. C.; Bach, U.; Cheng, Y.-B.; Simonov, A. N. Silver Bismuth Sulfoiodide Solar Cells: Tuning Optoelectronic Properties by Sulfide Modification for Enhanced Photovoltaic Performance. *Advanced Energy Materials* **2019,** *9* (5), 1803396.
(21) Li, T.; Hu, Y.; Morrison, C. A.; Wu, W.; Han, H.; Robertson, N. Lead-free pseudo-three-dimensional organic-inorganic iodobismuthates for photovoltaic applications. *Sustainable Energy & Fuels* **2017,** *1* (2), 308-316.
(22) Hu, Z.; Wang, Z.; Kapil, G.; Ma, T.; Iikubo, S.; Minemoto, T.; Yoshino, K.; Toyoda, T.; Shen, Q.; Hayase, S. Solution-Processed Air-Stable Copper Bismuth Iodide for Photovoltaics. *ChemSusChem* **2018,** *11* (17), 2930-2935.